COHERENT TRANSVERSE INSTABILITY OF A BUNCHED BEAM INDUCED BY INTERACTION WITH A KICKER MAGNET

Y. MIYAHARA and K. TAKATA

National Laboratory for High Energy Physics
Oho-machi, Tsukuba-gun, Ibaraki-ken, 300-32, Japan

Coherent transverse instabilities observed in the KEK booster have been studied experimentally and theoretically. The instabilities are induced by interaction of the beam with a ferrite-loaded kicker magnet. Here we consider the case when the matching resistance of the magnet is removed. There are some resonance frequencies in the magnet that contribute to the instability. The relation between the ac current passing through the magnet gap and the induced current in the coil is represented by a mutual inductance. A calculation is made of the field induced in the magnet by a bunched beam, the betatron oscillation of which is modulated by the synchrotron oscillation. The beam is regarded as a free string. The motion of the beam caused by the induced field is calculated and a formula for the buildup time of the oscillation amplitude is obtained in the form of an eigenvalue of a matrix equation. Numerical results agree quite well with the experiments in regard to the buildup time, the oscillation mode and the time of appearance of the instability during acceleration.

1. INTRODUCTION

Coherent transverse instability has been observed in many particle accelerators, accompanying increases of beam current. Theoretical and experimental studies have revealed the nature of the instability and given basic ideas for compensating systems. Laslett, Neil and Sessler[1] developed a theory of the instability for a coasting beam taking into account the resistive wall of vacuum chamber. Courant and Sessler[2] extended the theory to bunched beams. They treated each bunch as rigid and considered bunch-to-bunch interaction. This work showed that tune and tune spread were important factors for the instability. On the other hand, Pellegrini[3] and Sands[4] considered the interaction within the bunch, taking into account the coupling of the synchrotron and betatron oscillation. They showed that the instability depended on the bunch mode and the sign of the chromaticity. Sacherer[5] summarized these considerations and represented the mode explicitly. All these theories are very elaborate, but the agreement with the observations or experiments is not satisfactory. This is partly because it is difficult to calculate precisely the interaction of the beam with complex surrounding structures and partly because the source of the interaction is not always clear.

In the KEK booster we have observed a coherent transverse instability in the horizontal direction. It

has been proved[6] that the instability is induced by interaction between the beam and the kicker magnet which is used for fast beam extraction. The magnet is composed of laminations of ferrite cores and electric plates, so it responds to high-frequency beam oscillations. The one-turn coil of the magnet is terminated with a matched load resistance. When the termination is removed, the instability grows more rapidly. Here we confine ourselves to analysis of the instability for the case where the termination is removed. The kicker magnet without the termination resonates at some frequencies, which contributes to the instability. Therefore the treatment in this paper concerns essentially a transverse instability of a resonant type. As shown later, this includes the bunch-to-bunch interaction as well as the intra-bunch interaction.

As for the treatment of the bunched beam itself, we take into account the chromaticity in the same way as the theory of Pellegrini and Sands. However, unlike their treatment where they follow the forced motion of a given particle, we consider the motion of collective particles which arrive at the kicker magnet at the same time, and regard them as a short section of a free string. Every particle rotates in the rf bucket because of the synchrotron motion and the revolution period is modulated sinusoidally. Pellegrini and Sands formulated the motion of such a particle forced by the preceding particle within the bunch through some intervening surroundings. This treat-

ment is, however, not so convenient because of the oscillating period when we include the bunch-to-bunch interaction. This is especially so for a case when the reactor or the kicker magnet has some resonating periods. As described later, the particles that arrive at a given point at the same time have the same phase of betatron-oscillation amplitude with respect to the modulating phase of the synchrotron oscillation. We can therefore regard them as a section of a string whose revolution period is the same as the synchronous particles. We set aside the longitudinal movement of each particle within the bunch. This treatment is as if we were to consider the motion of a train (flexible) regardless of the movement of the passenger from car to car in the train, with the condition that the number of passengers in a given car remains constant.

In the booster ring, proton beam is accelerated from 20 MeV to 500 MeV in 25 msec with a harmonic number of 1; the revolution frequency changes from 1.6 MHz to 6.0 MHz. The number of the particles in the bunch is approximately 4 to 6 × 10^{11}. The accelerated beam is extracted by fast excitation of the kicker magnet. In normal operation of the kicker magnet, the instability is observed at 13 to 20 msec after the injection and the buildup time is 3 to 5 msec. When the termination of the magnet is removed, the instability is induced at approximately 17 msec and the buildup time is 1 to 2 msec.

In the following, we give first the characteristics of the kicker magnet in section 2. The interaction between ac current and the magnet is represented by a mutual inductance and the induced field due to the current is derived. In section 3, the reaction of the bunched beam to the field induced by the beam itself is calculated. The buildup time of the instability is shown to be given by an eigenvalue of a matrix equation. In section 4, numerical calculations are made and the results are compared with the observations and experiments. The agreement is very good. Finally some discussion is given in section 5.

2. CHARACTERISTICS OF THE KICKER MAGNET

2-1 Equivalent circuit of the kicker magnet

For the purpose of fast extraction of the accelerated proton beam, three identical kicker magnets are installed in a straight section of the booster ring. The parameters of the magnet are given in Table 1.[7]

Since the magnetic field is required to build up

TABLE 1

Parameters of kicker magnets

total length	l_B	300 mm
number of sections	N	12
gap height	h	40 mm
aperture	w	100 mm
inductance (per section)	L	7.85×10^{-8} H
capacitance (per section)	C	155×10^{-12} F
characteristic impedance	Z_0	22.5 Ω

very rapidly (in order of 50 nsec), the structure of the magnet is different from usual magnets. It has 12 sections, each of which is composed of a ferrite core and capacitive electrode. Its equivalent circuit is expressed by the lumped LCR circuit shown in Fig. 1. With respect to the n-th mesh, the following relation holds for the voltage V_n and current I_n,

$$V_n - L\dot{I}_n - RI_n - V_{n+1} = 0. \quad (2\text{-}1)$$

Since $\dot{V}_n = (I_{n-1} - I_n)/C$, we obtain

$$\Omega^2(I_{n-1} + I_{n+1} - 2I_n) - \delta\dot{I}_n - \ddot{I}_n = 0, \quad (2\text{-}2)$$

where $\Omega = 1/\sqrt{LC}$ and $\delta = R/L$. With the boundary conditions $I_0 = I_N = 0$, the solution of these equations can be easily obtained;

$$I_n = 2jA \sin\left(\frac{mn\pi}{N}\right) e^{j\Omega_m t - (\delta/2)t}, \quad (2\text{-}3)$$

with

$$\Omega_m = \Omega_m^0 \sqrt{1 - \left(\frac{\delta}{2\Omega_m^0}\right)^2}, \quad (2\text{-}4)$$

$$\Omega_m^0 = 2\Omega \sin\left(\frac{m\pi}{2N}\right) \quad (m = 1 \text{ to } N),$$

where m is the resonance mode. There are $N\,(=12)$ resonance frequencies, which are $\Omega_1/2\pi \approx 12$, $\Omega_2/2\pi \approx 24$, $\Omega_3/2\pi \approx 35\ldots$MHz, obtained by substituting numerical values in Table 1.

We have measured the resonance frequency by the method shown in Fig. 2. The results are shown in Fig. 3. At resonance frequencies the voltages V_0 and V_N at the both ends in the equivalent circuit become large. The frequency dependences of V_0 and V_N are the same. The measured resonance frequencies are
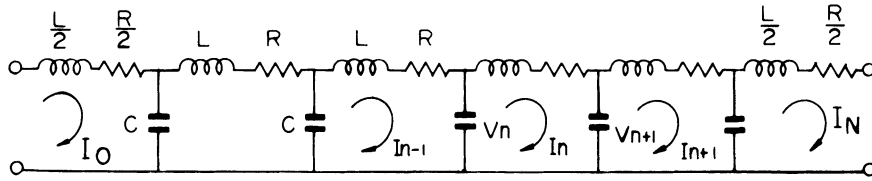
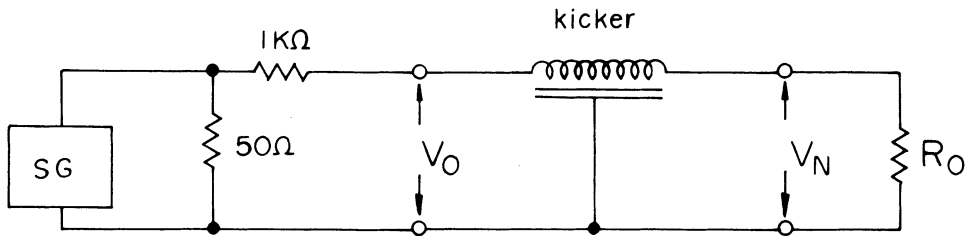FIGURE 1   Equivalent circuit of the kicker magnet.

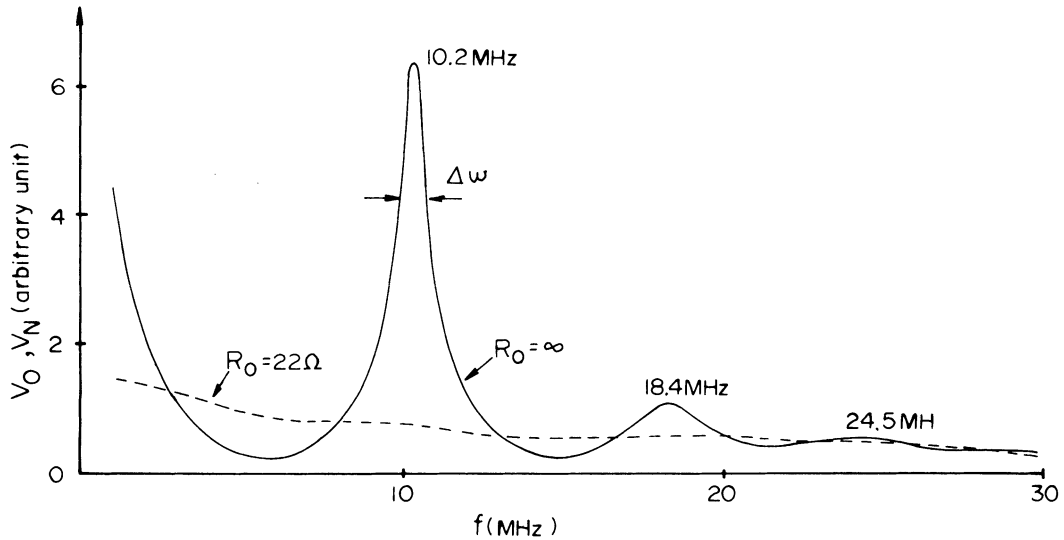FIGURE 2   Method of measuring the resonance frequency of the kicker magnet.

FIGURE 3   Frequency dependence of V_0 or V_N. The resistance R_0 ($= 22\Omega$) is the matched load.

10.2, 18.4, 24.5,...MHz, which do not agree well with those calculated. This may be due to the simplicity of the equivalent circuit. The disagreement does not much matter for consideration of the instability. By applying the relation $Q = \Omega_m/\Delta\omega$ $= \Omega_m L/R$, the resistance R is estimated to be 0.4 Ω, 1.2 Ω and 3 Ω for the peaks at 10.2 MHz, 18.4 MHz and 24.5 MHz, respectively. Here Q is the quality factor and $\Delta\omega$ is the frequency width of the resonance. The damping time of the large peak at 10.2

MHz is approximately $\tau_d \simeq 1/\Delta\omega \simeq 0.2\ \mu s$. This is nearly the same as the revolution period around 17 msec after injection, when the instability is observed.

2-2 Field induced in the kicker magnet by a sinusoidal current

As described in section 1, the circulating beam induces electric and magnetic fields in the gap of the kicker magnet, to which the beam reacts and becomes unstable in some conditions. In order. to investigate the field induced in the gap, we have measured the induced current i_2 in the one-turn coil of the magnet when a sinusoidal current i_1 flows through a wire stretched through the gap of the magnet. The ends of the coil are connected by a resistance R_2 with which the induced current was monitored. First the ratio $|i_2/i_1|$ was measured as a function of the position Δx of the primary current in the gap at 800 kHz. This is low enough compared with the resonance frequencies so that the induced current runs almost totally through R_2 and L. The result is shown with solid circles in Fig. 4. The induced current decreases linearly with increasing Δx. Next the frequency dependence of $|i_2/i_1|$ was measured at $\Delta x = 0$ or at the center of the gap. The result is shown with solid circles in Fig. 5. The induced current increases linearly with increasing frequency. The phase difference between the two currents is 90° in the frequency range 0.1 to 3 MHz. These characteristics clearly indicate that the secondary current is induced by the alternating magnetic flux passing through the ferrite cores. If electrostatic induction were dominant, the induced current would be zero at $\Delta x \approx 0$ and almost independent of frequency. The relation of the two currents can then be expressed with a mutual inductance. At higher frequencies, comparable to the resonance frequencies, the induced current passes through the capacitance C.

Next we calculate the mutual inductance M per unit section. By definition $M = \phi/i_i$, where ϕ is the flux induced by i_i in the area enclosed by the coil. A computer program calculation was made of the magnetic field induced by dc current passing at various positions Δx. Figure 6 is an example of the field distribution at the median plane. The flux enclosed in the coil is indicated by the dotted area, taking into account the skin effect. For ac current of sufficiently high frequency, the flux is inhibited from penetrating inside the coil itelf. It therefore seems appropriate to set the boundary of the dotted area as

shown in the figure. The calculated mutual inductance per unit section for various Δs is well represented by

$$M = \{10.1 - 0.160\ \Delta x(\text{mm})\}$$
$$\times 10^{-8}\ [\text{Tesla m}^2/A] \qquad (2\text{-}5)$$

The equivalent circuit of the primary and secondary currents at low frequencies is represented in Fig. 7-a. The following relation holds between the two currents:

$$2R_2 i_2 + N(Ri_2 + L\dot{i}_2 + M\dot{i}_1) = 0. \ (2\text{-}6)$$

For a primary current $i_1 = I_p e^{j\omega i}$, the secondary current is given by

$$i_2 = I_s e^{j[\omega t + (\pi/2) + \theta]},$$

where

$$\theta = \text{arc tan}\left[-\left(\frac{\omega NL}{2R_2 + NR}\right)\right] \quad (R_2 \gg R),$$
$$(2\text{-}7)$$

$$|i_2/i_1| = -\frac{\omega NM}{(2R_2 + NR)\cos\theta - \omega NL\ \sin\theta}$$

On substituting numerical values, $|i_2/i_1|$ is represented by straight lines in Figs. 4 and 5. Agreement of the calculation with measured values is very good.

2-3 Induced currents at high frequencies

We now consider forced oscillations in the resonance-frequency range in the equivalent circuit of Fig. 7-b. The same mutual inductance given in Eq. (2-5) is valid for these frequencies. As before, there is a relation for the n-th mesh:

$$\Omega^2(I_{n-1} + I_{n+1} - 2I_n) - \delta\dot{I}_n - \ddot{I}_n = -\gamma\ddot{i}_1, \quad (2\text{-}8)$$

where $\Omega = 1/\sqrt{LC}$, $\delta = R/L$, $\gamma = M/L$ and $i_1 = i_0 e^{j\omega t}$. Since several low resonance frequencies will be seen to be related to the instability, we solve Eq. (2-8) with a smooth approximation. Let I_n be replaced by $I(z)$, where $z = nd$ and d is the length of a unit section, and take the differences. Then

$$I_{n-1} + I_{n+1} - 2I_n = d^2\ \frac{\partial^2 I(z)}{\partial z^2}, \qquad (2\text{-}9)$$

so that Eq. (2-8) becomes

$$\Omega^2 d^2\ \frac{\partial^2 I(z,t)}{\partial z^2} - \delta\dot{I}(z,t) - \ddot{I}(z,t) = i_0\gamma\omega^2 e^{j\omega t}.$$
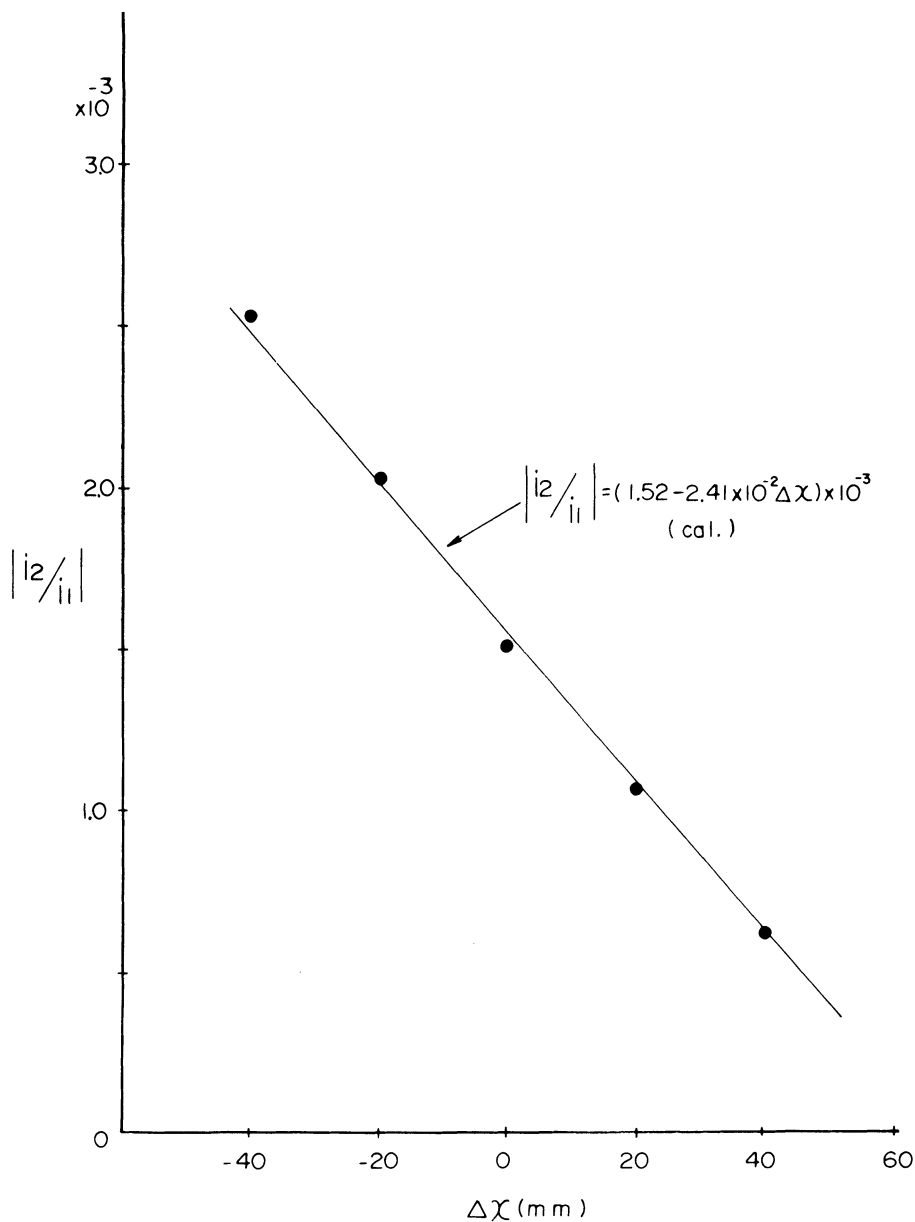$$(2\text{-}10)$$

FIGURE 4   Ratio of the secondary current to the primary current $|i_2/i_1|$ versus the position of the primary current Δx. The solid marks are experimental and the straight line is theoretical.

Keeping in mind the boundary condition $I_0 = I_N = 0$, we expand $I(z,t)$ in a Fourier series

$$I(z,t) = \sum_{m=1}^{\infty} Y_m(t) \sin\left(\frac{m\pi z}{l_B}\right) , \quad (2\text{-}11)$$

where $l_B = (= Nd)$ is the total length of the kicker magnet. Although the right-hand side of Eq. (2-10) is independent of z, we expand it similarly for a technical purpose;

$$i_0\gamma\omega^2 e^{j\omega t} = \sum_{m=1}^{\infty} f_m(t)\sin\left(\frac{m\pi z}{l_B}\right). \quad (2\text{-}12)$$
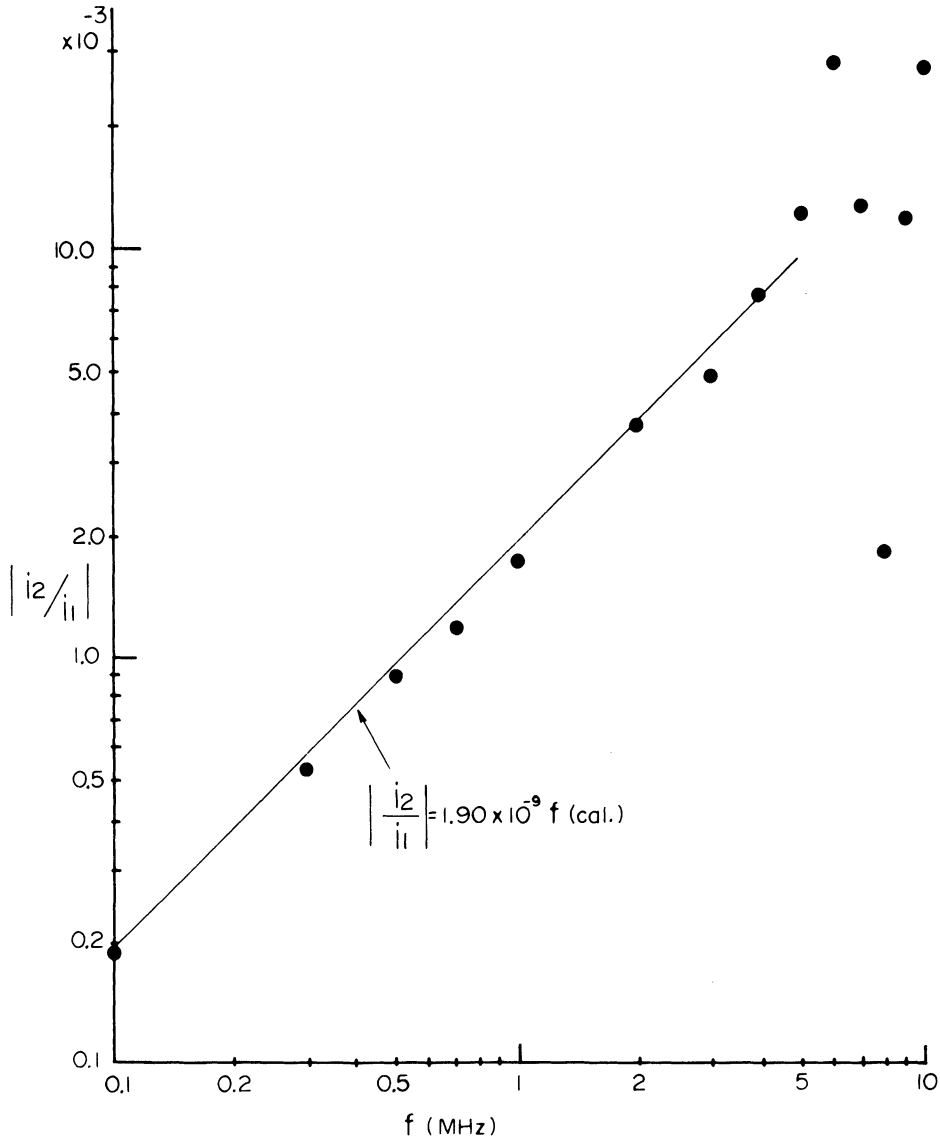
FIGURE 5   Ratio $|i_2/i_1|$ versus the frequency of the primary current. The solid marks are experimental and the straight line is theoretical.

By the reverse transformation we get

$$f_m(t) = \begin{cases} \dfrac{4i_0\gamma\omega^2}{m} \; e^{j\omega t}, & \text{for } m = 1, 3, 5 \ldots \\ 0, & \text{otherwise.} \end{cases} \quad (2\text{-}13)$$

Substituting Eqs. (2-11) and (2-12) into Eq. (2-10), we get

$$\ddot{Y}_m(t) + \delta\dot{Y}_m(t) + \Omega_m^2 Y_m(t) = -f_m(t), \quad (2\text{-}14)$$

where $\Omega_m = \Omega m/N$, which is slightly different from Eq. (2-4), but agrees in the low-frequency limit. The solution of the equation (2-14) is easily obtained;

i) for $m = 2, 4, 6, \ldots$ $(f_m(t) = 0)$

$$Y_m(t) = e^{-\delta t/2} (Ae^{\delta mt} + Be^{-\delta mt}), \quad (2\text{-}15)$$

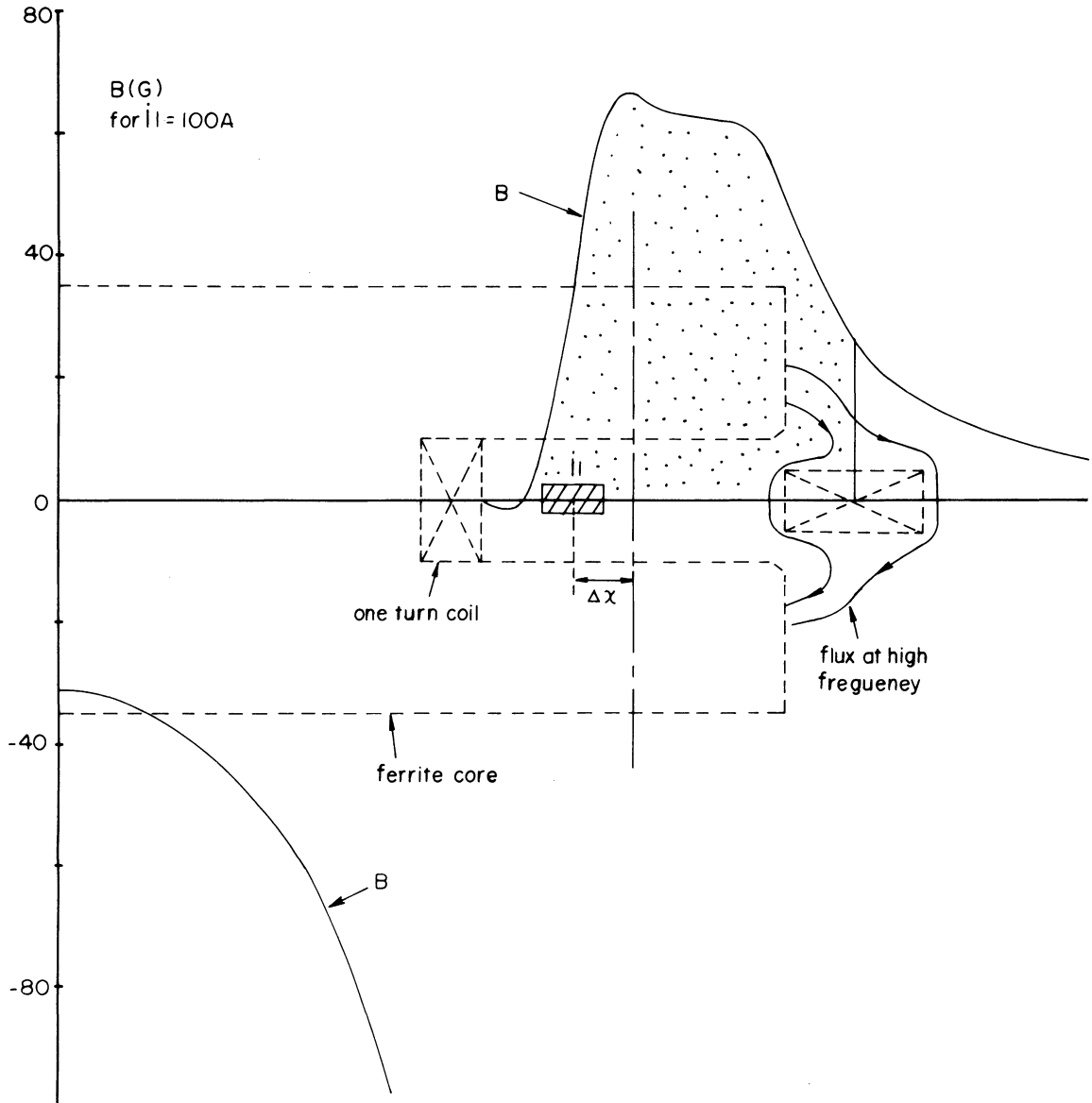where $\delta m = ((\delta/2)^2 - \Omega_m^2)^{\frac{1}{2}}$.

FIGURE 6   Magnetic field at the median plane induced by the primary current i_1.

$Y_m(t)$ always damps regardless of the sign of $[(\delta/2)^2 - \Omega_m^2]$.

ii) for $m = 1, 3, 5, \ldots (f_m(t) \neq 0)$

$$Y_m(t) = A_m \, e^{j(\omega t + \alpha_m)} \qquad (2\text{-}16)$$

$$A_m = \frac{4i_0\gamma}{m\pi} \frac{\omega^2}{\sqrt{(\omega^2 - \Omega_m^2)^2 + (\omega\delta)^2}} \qquad (2\text{-}17)$$

and

$$\alpha_m = \arctan\left(\frac{\omega\delta}{\omega^2 - \Omega_m^2}\right) . \qquad (2\text{-}18)$$
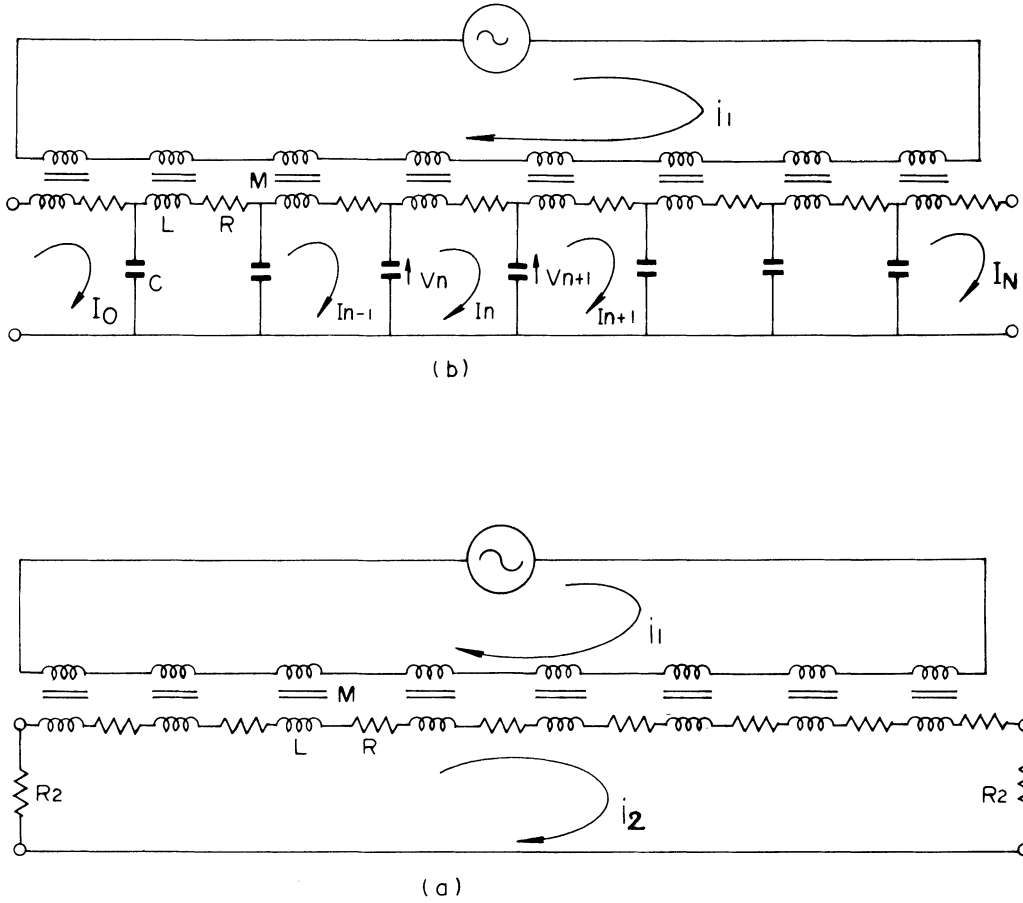
FIGURE 7   Equivalent circuit of kicker magnet with the primary current at low frequency (a) and at high frequency (b).

Figure 8 represents the frequency dependence of the amplitude A_m and the phase lag α_m for typical values of R. For the resonance frequencies Ω_m we use the measured values shown in Fig. 3. Near the resonance frequencies, the amplitude becomes large and the phase lag rapidly crosses $\alpha_m = -90°$. Comparing the peak widths in Figs. 3 and 8, we see that the resistances R previously estimated for each resonance frequency from Fig. 3 have reasonable values. It is noteworthy that the phase lag is an important factor in the buildup of the instability.

3. INTERACTION BETWEEN BUNCHED BEAM AND KICKER MAGNET

3-1 String model of bunched beam

The betatron-oscillation frequency per revolution ν deviates in proportion to the deviation of the mo-

mentum of the particle;

$$\frac{\Delta \nu}{\nu} = \zeta \frac{\Delta p}{p} ,   \quad (3\text{-}1)$$

where ζ is the chromaticity. Because of the synchrotron motion of a particle in the rf bucket, $\Delta \nu / \nu$ also makes synchrotron oscillations. Therefore a phase shift in the betatron oscillation is brought about by the synchrotron oscillation. The betatron-oscillation amplitude of the l-th particle is given by[4]

$$\Delta x_l = Z_l' e^{j\omega\beta(t+\eta'\tau'_l)},   \quad (3\text{-}2)$$

where Z_l' is the oscillation amplitude, $\omega_\beta/2\pi$ is the betatron-oscillation frequency without synchrotron modulation, τ_l' is the time of arrival at a given point in advance of the synchronous particle and $\eta' = 1 - (\zeta/\eta)$. Because of the velocity of the particle $\beta \neq 1, \eta = \alpha - (1/\gamma^2)$, where α is the momentum-com-
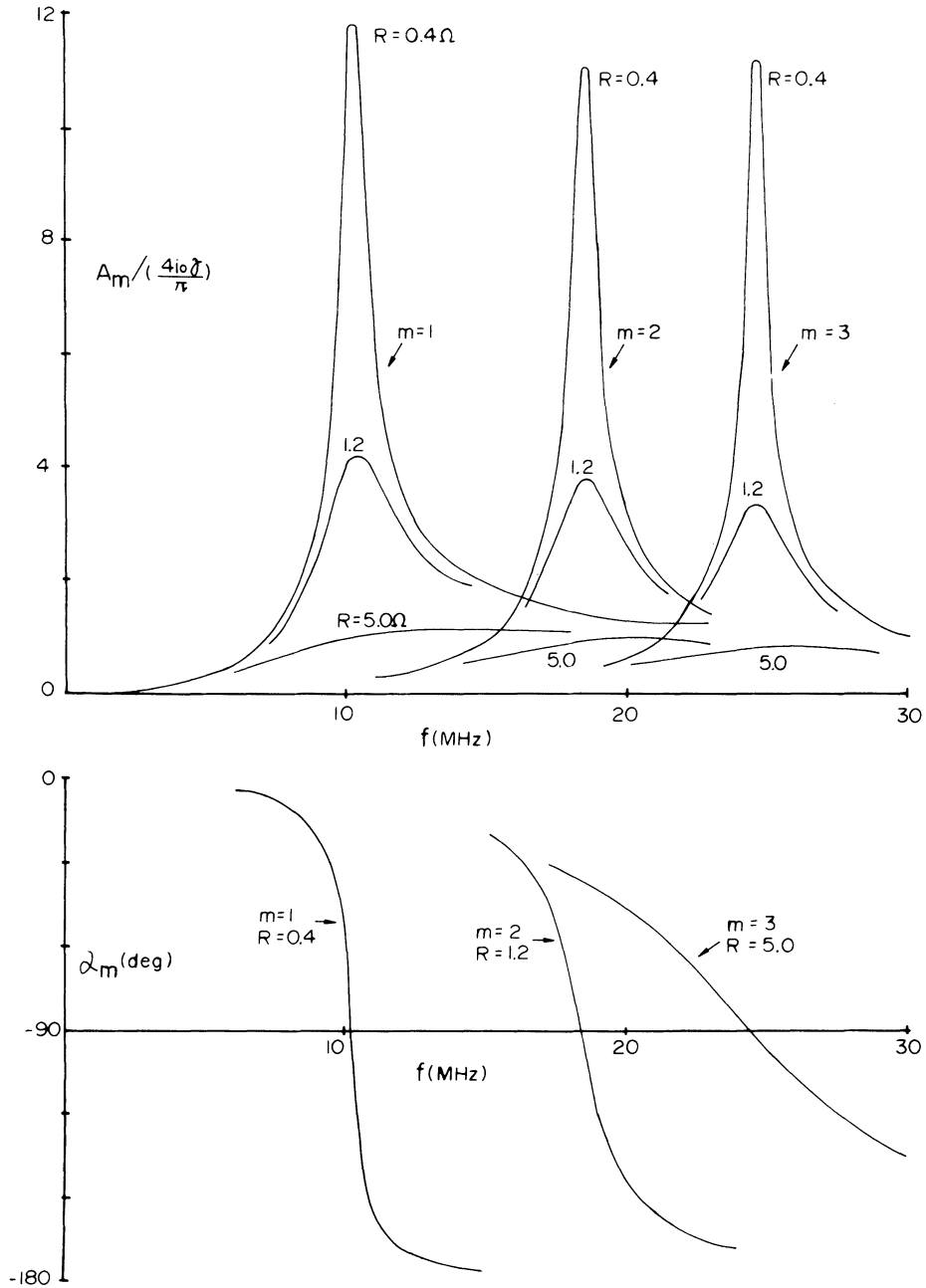
FIGURE 8   Frequency dependence of the amplitude A_m and the phase lag α_m.

paction factor, and $\gamma = 1/(1 - \beta^2)^{\frac{1}{2}}$. By replacing τ_l' by $-\tau_l$ and $Z_l'^{-j\omega\beta\tau_l}$ by Z_l in Eq. (3-2), we find

$$\Delta x_l = Z_l e^{j(\omega\beta t + \omega\zeta\tau_l)}, \qquad (3\text{-}3)$$

where $\omega_\zeta = (\zeta/\eta)\omega_\beta$. The quantity τ_l changes

sinusoidally with time and the l-th particle moves forward and backward in the bunch.

There are other particles than the l-th particle whose synchrotron-oscillation amplitudes are different. Note that these particles have the same phase $\omega_\zeta\tau_l$ with respect to modulation by the synchrotron

oscillations since Δx_l in Eq. (3-3) is independent of $\Delta p/p$. Therefore, by neglecting the longitudinal motion of each particle, we can regard the particles that arrive at the same time as a short section of a charged free string. We do not follow the motion of a given particle, but consider instead the motion of the short section of the string. The revolution period is the same for all sections. In spite of the synchrotron motions of individual particles, the longitudinal distribution is constant with respect to the time. Thus we give the distribution to the string.

3-2 Field induced by bunched beam

First we consider the field induced in the kicker magnet by the l-th section, which makes the betatron oscillation described by Eq. (3-3). The section passes through the magnet at the time $t = nT + \tau_l$, where n is an integer and T is the revolution period. The current of this section at the magnet is

$$i_l = i_0 \rho_l D(t - nT - \tau_l), \qquad (3-4)$$

where ρ_l is the normalized charge density and

$$D(t - nT - \tau_l) = \begin{cases} 1 & \text{for } nT + \tau_l < t < nT \\ & \qquad + \tau_l + \Delta\tau_l \\ 0 & \text{otherwise}, \end{cases} \qquad (3-5)$$

where $\Delta\tau_l$ is the time length of the l-th section. The function D can be expanded in a Fourier series; that is,

$$D(t - nT - \tau_l) = \frac{1}{T} \sum_{k=-\infty}^{\infty} e^{jk\omega_0(t - \tau_l)\Delta\tau_l}, \qquad (3-6)$$

where $\omega_0 = 2\pi/T$. Taking into account the previous description in section 2-3, the magnetic flux induced by the l-th section within the coil of the magnet is

$$\phi_l = (a - b\Delta x_l)i_l, \qquad (3-7)$$

where a and b are the coefficients given in Eq. (2-5). Note that the time dependence of $\phi_l(t)$ arises from $i_l(t)$ and $\Delta x_l(t)$. As described in section 2-3, the induced current in the magnet obeys the relation

$$\Omega^2(I_{n-1} + I_{n+1} - 2I_n) - \delta\dot{I}_n - \ddot{I}_n = -(1/L)\ddot{\phi}_l. \qquad (3-8)$$

From Eqs. (3-4), (3-6), and (3-7) we find

$$\ddot{\phi}_l = -\frac{ai_0}{2} \frac{\Delta\tau_l}{T} \sum_{k=-\infty}^{\infty} \rho_l(k\omega_0)^2 e^{-jk\omega_0\tau_l} e^{jk\omega_0 t}$$

$$-\frac{bi_0}{2} \frac{\Delta\tau_l}{T} \sum_{k=-\infty}^{\infty} \rho_l\{\ddot{Z}_l + 2j(k\omega_0 + \omega_\beta)\dot{Z}_l$$

$$- (k\omega_0 + \omega_\beta)^2 Z_l\}$$

$$\times e^{j(-k\omega_0 + \omega_\zeta)\tau_l} e^{j(k\omega_0 + \omega_\beta)t} \qquad (3-9)$$

As derived previously, the solution of Eq. (3-8) is given by

$$I(z,t) = \sum_{m=1,3,5,\ldots} \sum_{k=-\infty}^{\infty} \{Y_{mk}^a(t) + Y_{mk}^b(t)\}$$

$$\times \sin\left(\frac{m\pi}{l_B} z\right) \qquad (3-10)$$

where

$$Y_{mk}^{a,b}(t) = A_{mk}^{a,b} e^{j(\omega_k t + \alpha_{mk}^{a,b})}$$

$$A_{mk}^{a,b} = \frac{4}{m\pi} \frac{\Gamma_k^{a,b}}{\sqrt{(\omega_k^2 - \Omega_m^2)^2 + (\omega_k\delta)^2}}$$

$$\alpha_{mk}^{a,b} = \arctan\left(\frac{\omega_k\delta}{\omega_k^2 - \Omega_m^2}\right) \qquad (3-11)$$

$$\Gamma_k^a = \frac{ai_0}{2L} \frac{\Delta\tau_l}{T} \rho_l \omega_k^2 e^{-jk\omega_0\tau_l}$$

$$\Gamma_k^b = \frac{bi_0}{2L} \frac{\Delta\tau_l}{T} \rho_l\{\ddot{Z}_l + 2j\omega_k\dot{Z}_l - \omega_k^2 Z_l\}$$

$$\times e^{j(-k\omega_0 + \omega_\zeta)\tau_l}$$

and

$$\omega_k = k\omega_0 \qquad \text{for superscript } a$$

$$k\omega_0 + \omega_\beta \quad \text{for superscript } b.$$

The induced current $I(z,t)$ is distributed like $\sin(mz/l_B)$ in the coil of the magnet. The magnetic field produced by this current changes direction locally within the magnet depending on the sign of the current. Since the magnet length is very short compared with the wavelength of the betatron oscillation, only the average field contributes to the kick angle of the particle. The average current is given by

$$\langle I(z,t)\rangle = \sum_{m=1,3,5,\ldots} \sum_k (Y_{mk}^a + Y_{mk}^b) \frac{2}{m\pi} \qquad (3-12)$$

Here again we see that only odd m's are effective.

3-3 Equation of motion

In the previous section we have derived the induced current due to the l-th section. Here we consider the motion of the s-th section in reaction to the current. The sum of the magnetic fields produced by all sections exerts force on the s-th section at a time $t = nT + \tau_s$ (n: integer). Keeping in mind that the betatron frequency is almost unaffected, as will be shown later, the equation of motion of the s-th section is given by

$$\ddot{x}_s + \omega_\beta^2 x_s = \frac{f(t)}{m_0\gamma} D(t - nT - \tau_s), \qquad (3\text{-}13)$$

$$f(t) = \frac{ev\mu_0}{h} \sum_l <I(z,t)>,$$

where e is the unit charge, v the particle speed, h the magnet gap and m_0 the proton mass. Using expressions for the s-th section similar to Eqs. (3-3) and (3-5), we get from Eqs. (3-12) and (3-13)

$$(\ddot{Z}_s + 2j\omega_\beta \dot{Z}_s) e^{j(\omega_\beta t + \omega_\zeta \tau_s)}$$

$$= \frac{ev\mu_0}{m_0\gamma h} \sum_l \sum_m \sum_k \frac{1}{m\pi} (Y_{mk}^a + Y_{mk}^b) \frac{\Delta\tau_s}{T}$$

$$\sum_n e^{jn\omega_0(t-\tau_s)}. \qquad (3\text{-}14)$$

Note that $\Delta\tau_s$ in Eq. (3-14) is not the section length as before, but the time required for the section to pass through the magnet. Therefore $v\Delta\tau_s = l_B$. Since we consider a slow change of Z_s, we neglect $\dot{Z}_s$ and $\ddot{Z}_l$ in Eqs. (3-14) and (3-11).

If the contribution of the Y_{mk}^a term is dominant, then

$$2j\omega_\beta \dot{Z}_s e^{j(\omega_\beta t + \omega_\beta \tau_s)} \propto \sum_n \sum_k e^{j(k+n)\omega_0 t} \qquad (3\text{-}15)$$

Since v is not an integer,

$$\omega_\beta = v\omega_0 \neq (k + n)\omega_0; \qquad (3\text{-}16)$$

thus $Z_s(t)$ only oscillates. On the other hand, we get from Y_{mk}^b term

$$2j\omega_\beta \dot{Z}_s = (-) \frac{ev\mu_0}{m_0\gamma h} \frac{\Delta\tau_s}{T} \frac{bi_0}{2L} \sum_l \sum_m \sum_k \sum_n$$

$$\frac{8}{(m\pi)^2} \frac{\omega_k^2}{\sqrt{W_{mk}}}$$

$$\times \frac{\Delta\tau_l}{T} \rho_l Z_l e^{j(\omega_k + n\omega_0 - \omega_\beta)t}$$

$$\times e^{j(-k\omega_0 + \omega_\zeta)\tau_l} e^{-j(n\omega + \omega_\zeta)\tau_s} e^{j\alpha mk} \qquad (3\text{-}17)$$

where $\omega_k = k\omega_0 + \omega_\beta$, $W_{mk} = (\omega_k^2 - \Omega_m^2)^2 + (\omega_k\delta)^2$, and $\dot{Z}_l \ll \omega_k\tau_l$ is assumed. If $k + n \neq 0$,

$$Z_s \propto \exp[\exp j(k+n)\omega_0 t],$$

which simply oscillates. If $k+n = 0$, we get

$$\dot{Z}_s = j\sum_l \sum_m \sum_k H_{mk} Z_l \rho_l \Delta\tau_l e^{j(k\omega_0 - \omega_\zeta)(\tau_s - \tau_l)}, \qquad (3\text{-}18)$$

where

$$H_{mk} = \frac{2}{\omega_\beta} \frac{e\mu_0 l_B}{m_0\gamma h} \frac{1}{T^2} \frac{bi_0}{L} \frac{1}{(m\pi)^2} \frac{\omega_k^2}{\sqrt{W_{mk}}} e^{j\alpha mk}. \qquad (3\text{-}19)$$

This is the basic equation for the instability.

3-4 Solution of the basic equation

Since Z_s is a function of τ_s with period T, we can expand it in Fourier series,

$$Z_s = \sum_{n=-\infty}^{\infty} a_n e^{jn\omega_0\tau_s}. \qquad (3\text{-}20)$$

With this expansion, it is easier to make the calculation in Eq. (3-18). However the result does not explain explicitly the mode of the experimental observation (as described later). It is necessary to expand Z_s in the real series

$$Z_s = \sum_{n=0}^{\infty} \{a_n\sin(n\omega_0\tau_s) + b_n\cos(n\omega_0\tau_s)\}, \qquad (3\text{-}21)$$

where n is the mode number. Substituting this in Eq. (3-18), we have

$$\sum_n \{\dot{a}_n\sin(n\omega_0\tau_s) + \dot{b}_n\cos(n\omega_0\tau_s)\}$$

$$= j\sum_l \sum_m \sum_k \sum_p H_{mk} \rho_l \Delta\tau_l \{a_p\sin(p\omega_0\tau_l)$$

$$+ b_p\cos(p\omega_0\tau_l)\} \times e^{j(k-q)\omega_0(\tau_s - \tau_l)} \qquad (3\text{-}22)$$

where we have defined $q = \omega_\zeta/\omega_0$. We can solve for

$$\dot{a}_\mu(t) = - \sum_l \sum_m \sum_k \sum_p H_{mk}\rho_l\Delta\tau_l G_{\mu k}^-$$

$$\times \{a_p\sin(p\omega_0\tau_l) + b_p\cos(p\omega_0\tau_l)\}e^{-j(k-q)\omega_0\tau_l}, \qquad (3\text{-}23)$$

where

$$G^-_{\mu k} = g((\mu - k + q)\pi) - g((\mu + k - q)\pi)$$

and

$$g(y) = \sin y/y. \qquad (3\text{-}24)$$

Similarly we can find

$$\dot{b}_\mu(t) = j \sum_l \sum_m \sum_k \sum_p H_{mk}\rho_l\Delta\tau_l G^+_{\mu k}\{a_p\sin(p\omega_0\tau_l) + b_p\cos(p\omega_0\tau_l)\}e^{-j(k-q)\omega_0\tau_l}, \qquad (3\text{-}25)$$

where

$$G^+_{\mu k} = g((\mu - k + q)\pi) + g((\mu + k - q)\pi). \qquad (3\text{-}26)$$

Next we calculate the summation over l in Eqs. (3-23) and (3-25). The normalized charge distribution ρ_l along the orbit can be also expanded in Fourier series. But since we treat only the transverse instability, the density modulation is not important. Thus we approximate it as follows;

$$\rho_l = \begin{cases} \cos\left(\dfrac{\pi}{\tau}\tau_l\right) & \text{for } |\tau_l| \leq \tau/2 \\ 0 & \text{for } \tau/2 \leq |\tau_l| \leq T/2 \end{cases} \qquad (3\text{-}27)$$

Then the summation over l is

$$\sum_l = \int_{-\tau/2}^{\tau/2} \cos\left(\frac{\pi}{\tau}\tau_l\right)\{a_p\sin(p\omega_0\tau_l) + b_p\cos(p\omega_0\tau_l)\} \times e^{-j(k-q)\omega_0\tau_l}\,d\tau_l$$
$$= b_p F^+_{pk} - ja_p F^-_{pk}, \qquad (3\text{-}28)$$

where

$$F^\pm_{pk} = \frac{\pi\tau}{4}\{f((p-k+q)\pi r) \pm f((p+k-q)\pi r)\}$$
$$f(x) = \frac{\cos x}{\left(\dfrac{\pi}{2}\right)^2 - x^2} \qquad (3\text{-}29)$$

and $r = \tau/T$.

Equations (3-23) and (3-25) show that many modes couple together. We assume a unique time dependence for every mode;

$$a_\mu(t) = A_\mu e^{j\Delta\omega t}$$
$$b_\mu(t) = B_\mu e^{j\Delta\omega t} \quad (\mu = 0 \text{ to } \infty) \qquad (3\text{-}30)$$

Substituting these into Eq. (3-23) and using Eq. (3-28), we find

$$\Delta\omega \cdot A_\mu = j\sum_m \sum_k \sum_p H_{mk} G^-_{\mu k}(B_p F^+_{pk} - jA_p F^-_{pk}). \qquad (3\text{-}31)$$

Similarly from Eqs. (3-25) and (3-28)

$$\Delta\omega \cdot B_\mu = \sum_m \sum_k \sum_p H_{mk} G^+_{\mu k}(B_p F^+_{pk} - jA_p F^-_{pk}). \qquad (3\text{-}32)$$

Combining Eqs. (3-31) and (3-32), we get a matrix equation

$$\Delta\omega\begin{bmatrix} \vdots \\ A_\mu \\ \vdots \\ \vdots \\ B_\mu \\ \vdots \end{bmatrix} = \begin{bmatrix} \sum_m \sum_k H_{mk}G^-_{\mu k}F^-_{pk}, & j\sum_m \sum_k H_{mk}G^-_{\mu k}F^+_{pk} \\ & \\ -j\sum_m \sum_k H_{mk}G^+_{\mu k}F^-_{pk}, & \sum_m \sum_k H_{mk}G^+_{\mu k}F^+_{pk} \end{bmatrix}\begin{bmatrix} \vdots \\ A_p \\ \vdots \\ \vdots \\ B_p \\ \vdots \end{bmatrix} \qquad (3\text{-}33)$$

Thus $\Delta\omega$ is the eigenvalue of Eq. (3-33) and the A_p and B_p are elements of the eigenvector.

4. NUMERICAL CALCULATION AND COMPARISON WITH EXPERIMENTS

4-1 Method of the numerical calculation

The matrix equation (3-33) is of infinite dimension ($\mu, p = 0$ to ∞). It reduces to a small number of dimensions for realistic parameters of the booster and kicker magnet. As shown in Fig. 8, the functions A_m and H_{mk} become large at the resonance frequencies of the kicker magnet,

$$\omega_k = (k + \nu)\omega_0 = \Omega_m, \qquad (4\text{-}1)$$

where only odd m should be considered. The circulating beam meets many resonances during the acceleration ($\omega_0/2\pi = 1.6$ to 6.0 MHz), as indicated in Fig. 9. The resonance range of k for Ω_1 and Ω_3 is

$$-15 < k < 10. \qquad (4\text{-}2)$$

It is not necessary to consider higher resonance frequencies.

The functions $f(x)$ and $g(y)$ shown in Fig. 10 are both even functions. The function $f(x)$ decreases very rapidly with its argument; its effective range is
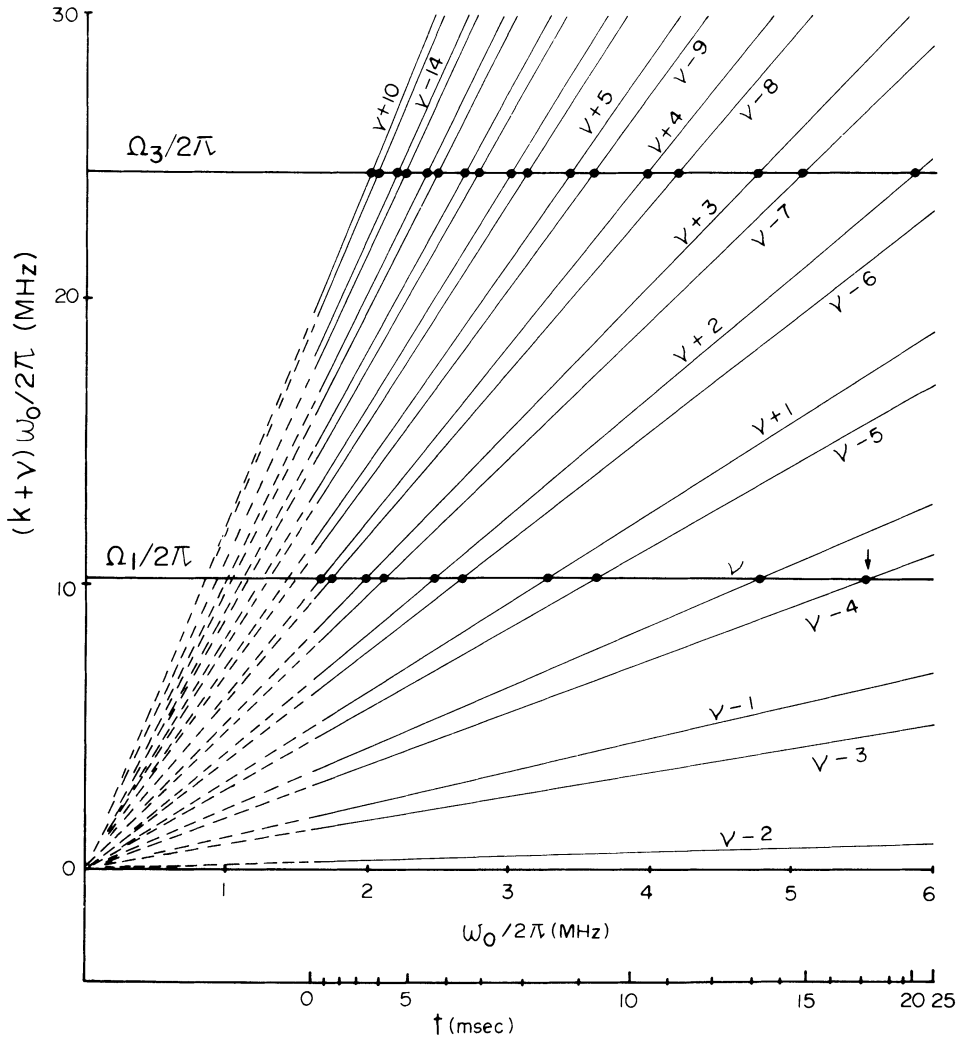
FIGURE 9   Resonance points that the beam meets during the acceleration. This figure is drawn for $\nu = 2.16$. Ω_1 and Ω_3 are the resonance frequencies of kicker magnet and ω_0 is the revolution frequency.

$$|x| \lesssim 3\pi, \qquad (4\text{-}3)$$

where $x = (p \pm (k - q))\pi r$.

The longitudinal charge distribution was observed with a fast intensity monitor and the ratio $r(= \tau/T)$ was obtained. The chromaticity of the booster was measured with the beam. The horizontal position of the beam was shifted with the rf feedback system and the ν value was measured. The chromaticity is obtained from the relation
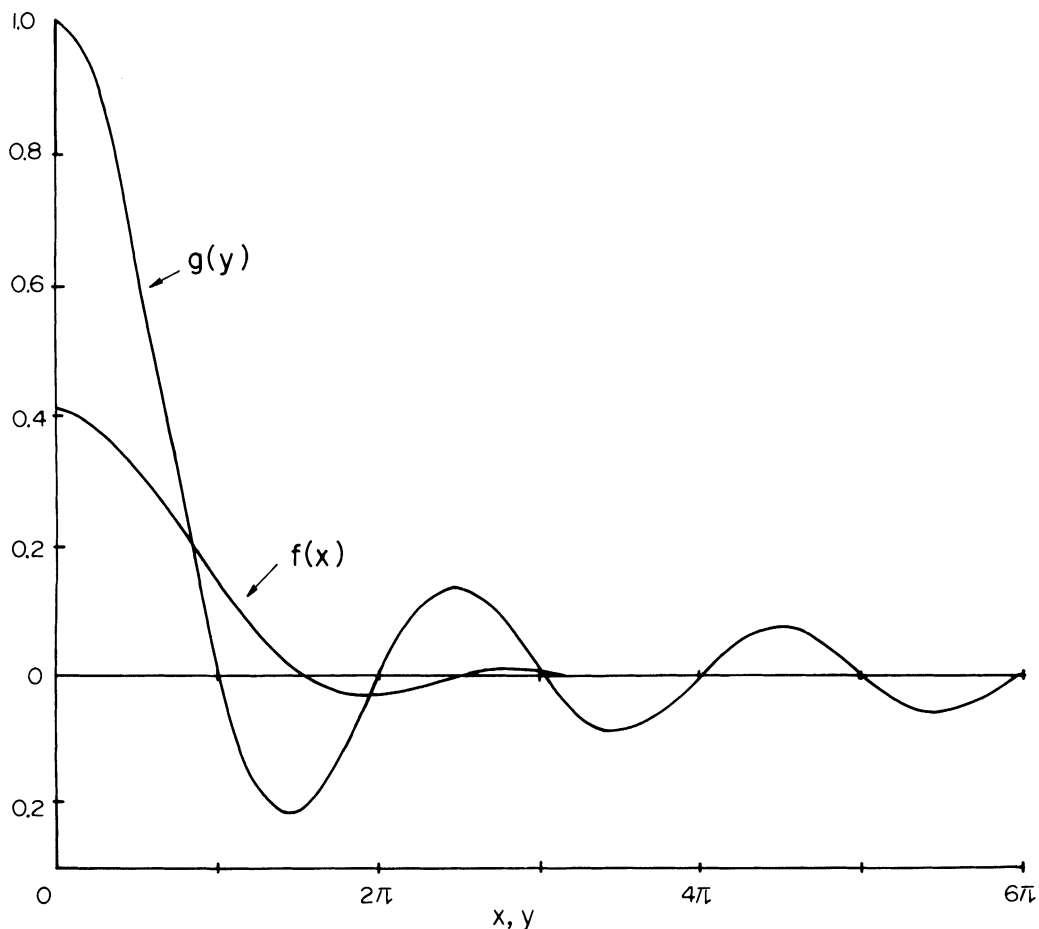
$$\zeta = \frac{x_p}{\nu} \frac{\Delta \nu}{\Delta x}, \qquad (4\text{-}4)$$

where x_p is the dispersion of the magnet. Then we get $q(= \omega_\zeta/\omega_0 = \zeta\nu/\eta)$. Figure 11 shows r and q as well as ζ and ν. The range of q is -1.5 to 3 and $r \simeq 0.5$. Then from Eqs. (4-2) and (4-3), the effective range of p is

$$0 \lesssim p \lesssim 24. \qquad (4\text{-}5)$$

Therefore the numerical calculation of Eq. (3-33) was made for dimensions $2D = 40$ to 60.

The numerical value of the proportional constant H_{mk} is given here.

FIGURE 10   Functions $f(x)$ and $g(y)$.

$$H_{mk} = \frac{\lambda}{v\gamma T\tau} \frac{1}{m^2} \frac{\omega_k^2}{\sqrt{(\omega_k^2 - \Omega_m^2)^2 + (\omega_k\delta)^2}} e^{j\alpha_{mk}},$$

$$\lambda = \frac{1}{2\pi^2} \frac{e^2\mu_0}{m_0} \frac{l_B bN}{hL} = 5.98 \times 10^{-5}. \quad (4\text{-}6)$$

Here we have set $N = 4.00 \times 10^{11}$ and used the relation

$$<I(t)> = eN\omega_0/2\pi$$

$$= \frac{1}{T} \int_{-\tau/2}^{\tau/2} i_0 \cos \left(\frac{\pi}{\tau} \tau_l\right) d\tau_l$$

$$= \frac{2}{\pi} \frac{\tau}{T} i_0. \quad (4\text{-}7)$$

4-2 Results of numerical calculations and comparison with experiment

i) buildup time of the instability   Now we have made computer calculations of the matrix equation (3-33). We set $\Delta\omega = \alpha - j\beta$. From Eq. (3-30), α gives the shift of the betatron-oscillation frequency and β the inverse of the buildup time of the oscillation amplitude. The oscillation is stable for $\beta \leqq 0$ and unstable for $\beta > 0$. For a matrix dimension $2D$, there are $2D$ eigenvalues, D of which are zero because G_{0k}^- and F_{0k}^- are zero. The results of the calculation is that almost every β is positive and the others are nearly zero. Figure 12 (K2) shows the maximum β_{max} at each acceleration stage. The highest peak of β_{max} appears around 17 msec. The buildup time corresponding to this peak is $\tau_l = 2.2$
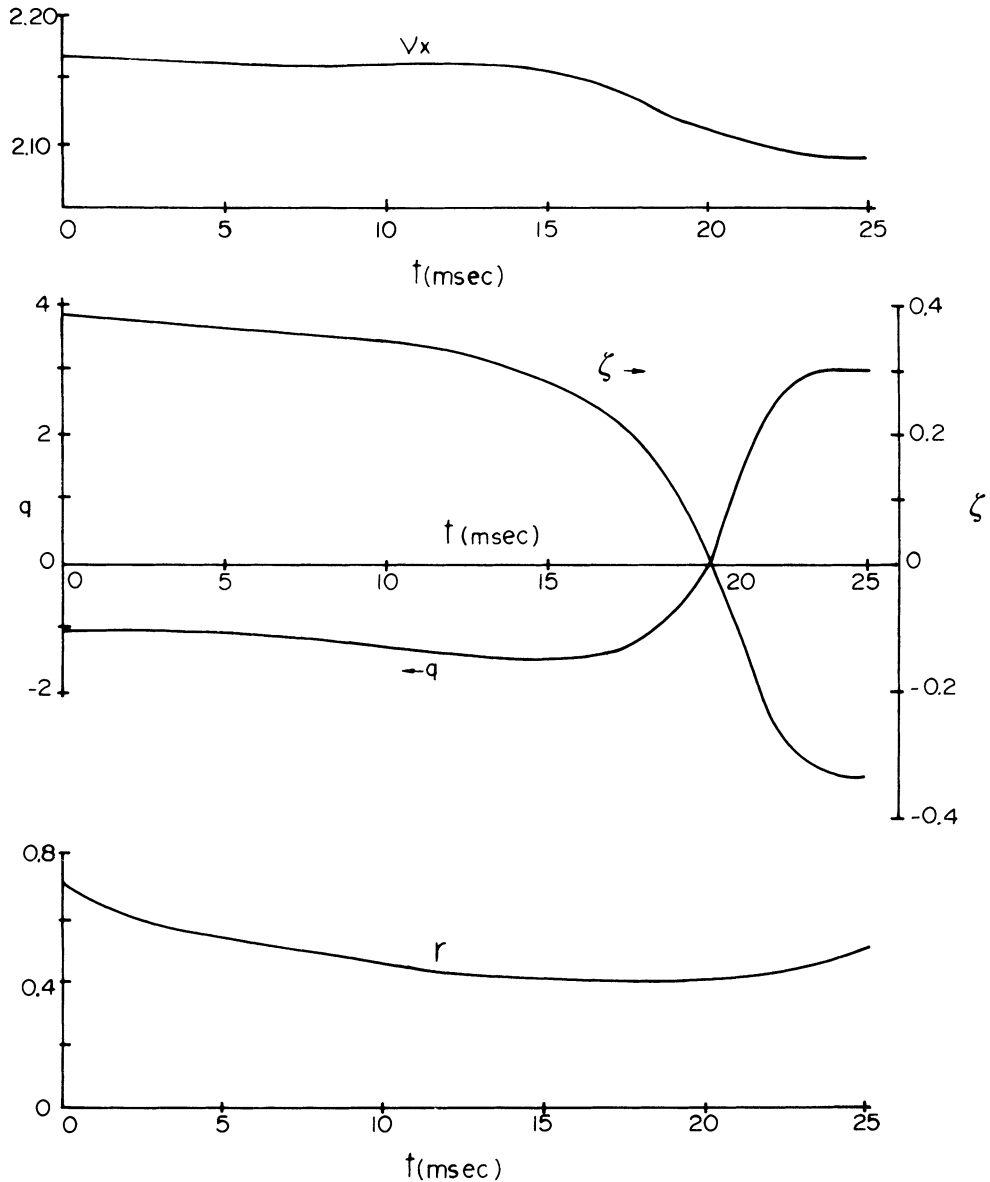
FIGURE 11   Measured r, q, ζ and v during the acceleration.

msec. This agrees with the appearance of the instability around 17 msec in the booster, as shown in Fig. 13-a. The observed buildup time is about 1 to 2 msec. The other peaks in Fig. 12 are lower and narrower, which explains why the instability is induced only near 17 msec. The peak at 17 msec corresponds to a resonance frequency $\Omega_1 = \omega_k = (-4 + v)\omega_0$ (see the arrow in Fig. 9). This peak is higher than the other peaks because H_{mk} is proportional to $1/T\tau$ or ω_0^2, as seen in Eq. (4-6). The other factors in Eq. (4-6), as well as $G_{\mu k}^{\pm}$ and $F_{pk}^{\pm}$, are not much different. The ω_0 is largest for the resonance point $k = -4$, as shown in Fig. 9. The higher resonance frequency Ω_3 does not much contribute because of the increasing m and δ or R.

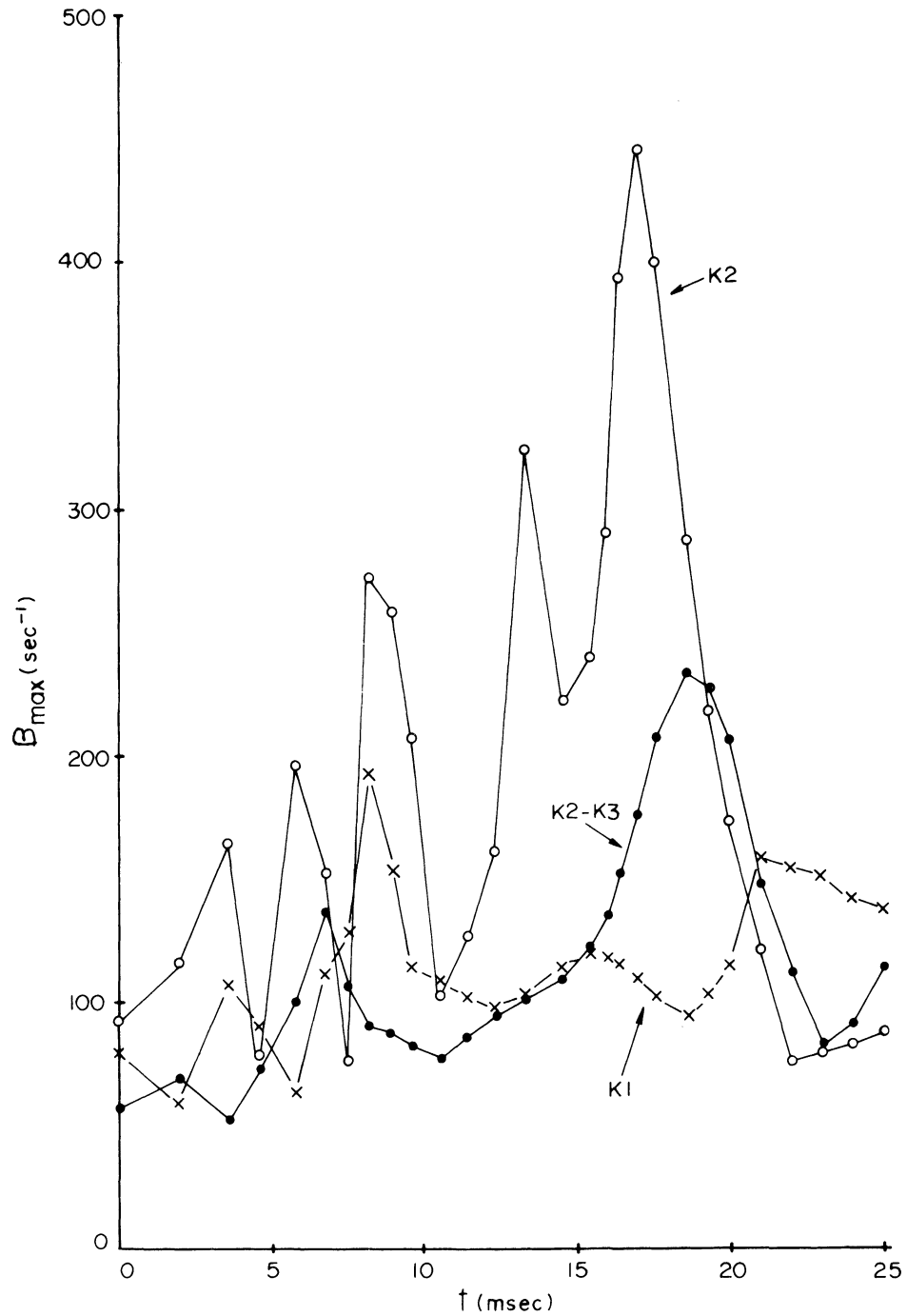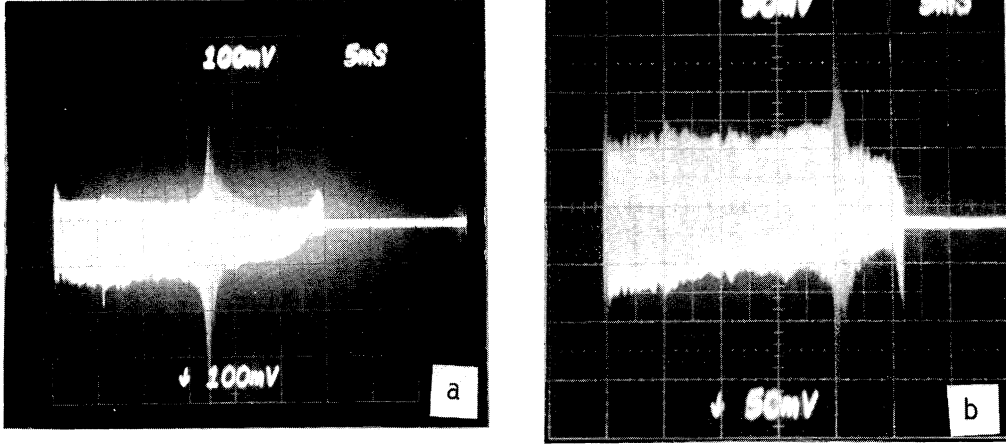When the terminations of more than one kicker

FIGURE 12   Build-up time during the acceleration. K2 is for the normal kicker magnet. K2–K3 is for the two coupled kicker magnets. K1 is for the other kicker magnet for single-turn injection test.

FIGURE 13 Horizontal ΔR signal of the booster beam; a for K2 and b for K1.

magnet are removed, the growth of the instability becomes more rapid. When the beam intensity is decreased the appearance of the instability becomes slow and delayed down to 18.5 msec.

The real part associated with β_{max} at 17 msec is $\alpha = -94 \ \text{sec}^{-1}$, so that the betatron frequency shift is only 10^{-6}. The eigenvector associated to β_{max} at 17 msec is

$$
\begin{bmatrix} A_0 \\ A_1 \\ A_2 \\ A_3 \\ A_4 \\ \vdots \\ B_0 \\ B_1 \\ B_2 \\ B_3 \\ B_4 \\ \vdots \end{bmatrix} = \begin{bmatrix} |X_\mu| & \theta_\mu \\ 0.000 & 0.695 \\ 0.178 & 1.186 \\ 0.649 & -0.565 \\ 1.000 & 0.000 \\ 0.169 & 0.070 \\ \vdots & \vdots \\ 0.476 & -0.475 \\ 0.679 & -0.584 \\ 0.819 & 0.403 \\ 1.000 & 0.092 \\ 0.511 & 1.244 \\ \vdots & \vdots \end{bmatrix} \qquad (4\text{-}8)
$$

where $X_\mu = |X_\mu| \ e^{i\theta}\mu$. The vector elements A_2 and A_3 or B_1, B_2 and B_3 are relatively larger. This is as expected because $f((p + k - q)\pi\gamma)$ and $g((\mu + k - q)\pi)$ are large for $p + k - q \approx 0$ and $\mu + k - q \approx 0$, which are satisfied near 17 msec for p or $\mu = 2$ and 3.

In order to see more intuitively we consider a special case of Eqs. (3-31) and (3-32). If only the A_μ

term is dominant, we get from Eq. (3-31)

$$
\Delta\omega = \sum_m \sum_k H_{mk} G^-_{\mu k} F^-_{\mu k}, \qquad (4\text{-}9)
$$

then by the definition $H_{mk} = Q_{mk} \ e^{j\alpha_{mk}}$,

$$
\alpha = \sum_m \sum_k Q_{mk} \cos\alpha_{mk} \ G^-_{\mu k} \ F^-_{\mu k} \qquad (4\text{-}10)
$$

$$
\beta = -\sum_m \sum_k Q_{mk} \sin \alpha_{mk} \ G^-_{\mu k} F^-_{\mu k}.
$$

Similarly, if the B_μ term is dominant,

$$
\Delta\omega = \sum_m \sum_k H_{mk} G^+_{\mu k} F^+_{\mu k}, \qquad (4\text{-}11)
$$

or

$$
\alpha = \sum_m \sum_k Q_{mk} \cos\alpha_{mk} \ G^+_{\mu k} F^+_{\mu k},
$$
$$
\beta = (-)\sum_m \sum_k Q_{mk} \sin\alpha_{mk} \ G^+_{\mu k} F^+_{\mu k}. \qquad (4\text{-}12)
$$

Near the resonance with the magnet ($\omega_k \approx \Omega_m$), Q_{mk} is large and $\sin\alpha_{mk} \approx -1$ and $\cos\alpha_{mk} \approx 0$, since $\alpha_{mk} \approx -\pi/2$. With the further condition $\mu(\geqq 0) \approx \pm(k-q) \approx 2.5$, $G^\pm_{\mu k} \cdot F^\pm_{\mu k}$ is large for $\mu = 2$ or 3.

ii) oscillation mode of ΔR signal The ΔR signal from a position monitor is proportional to the real part of $\rho_l \Delta x_l$;

$$
\Delta R_l \propto \sum_\mu \{A_\mu \cos(\pi\sigma_l)\sin(2\pi\mu\sigma_l)\cos 2\pi
$$
$$
\times (vn + qr\sigma_l) + B_\mu \cos(\pi\sigma_l)\cos(2\pi\mu\sigma_l)
$$
$$
\times \cos 2\pi(vn + qr\sigma_l)\}, \qquad (4\text{-}13)
$$

where $\sigma_l = \tau_l/\tau$ and $t = nT$ (n: integer). The oscillation mode μ is the μ-th coefficient of the
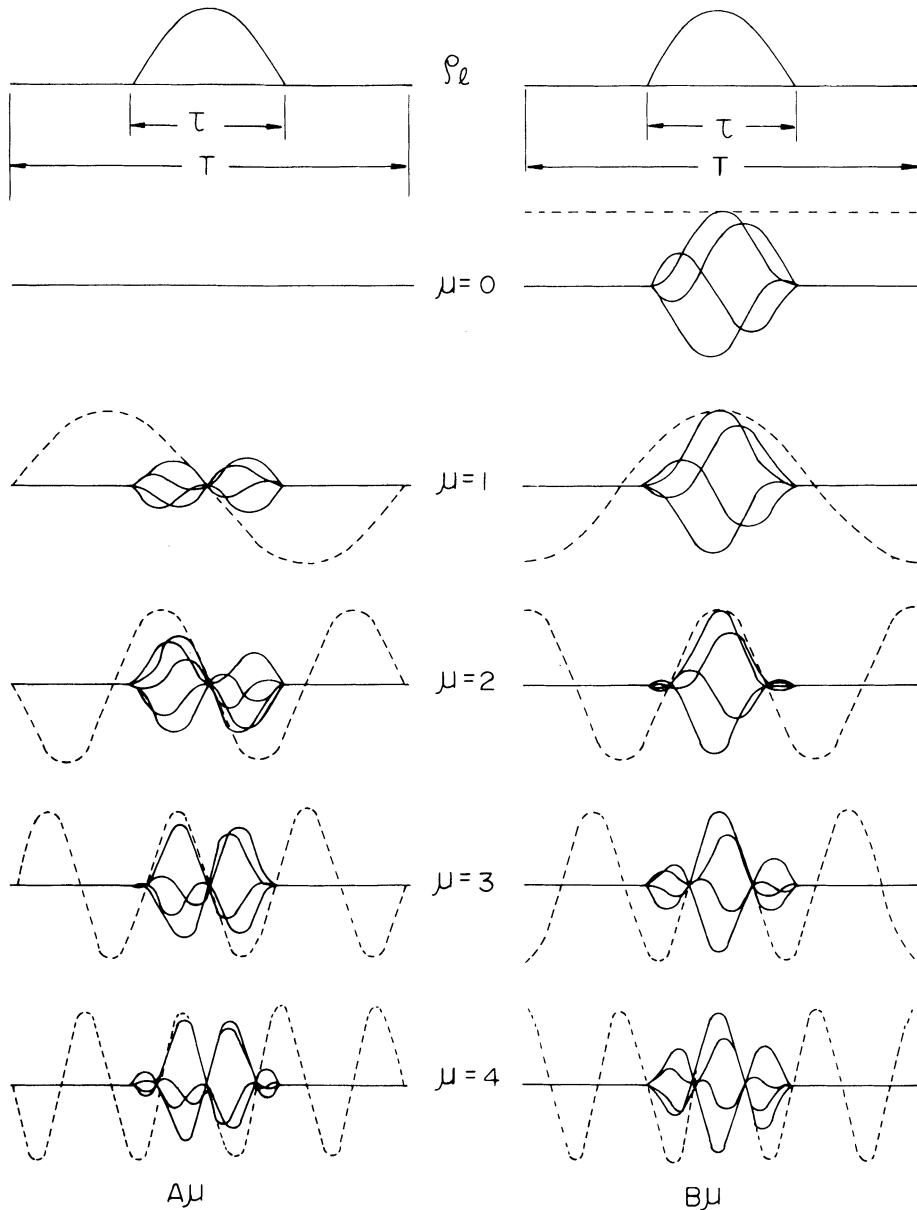
FIGURE 14   Calculated multi trace for various single modes (solid line). The broken lines are the mode representation. The left is the antisymmetric sin mode and the right is the symmetric cos mode.

Fourier expansion of Z_s, as given in Eqs. (3-21) and (3-30). Figure 14 shows the calculated multiple trace for various single modes. Coupled modes can be obtained by the linear combination of these single modes. Many modes which have been observed are the coupled modes, but some of them are single modes. Up to now we have observed several sym-

metric modes $\mu = (0, 1)$, (2), $(3$ or $4)$ and the antisymmetric modes $\mu = (1, 2$ or $3)$ as shown in Fig. 15. The observation of these modes is consistent with the eigenvector of Eq. (3-41). Figure 16 shows the subsequent multi-traces with a step of 1 msec in the range 18 to 21 msec. Induced single modes do not persist during the unstable region, but
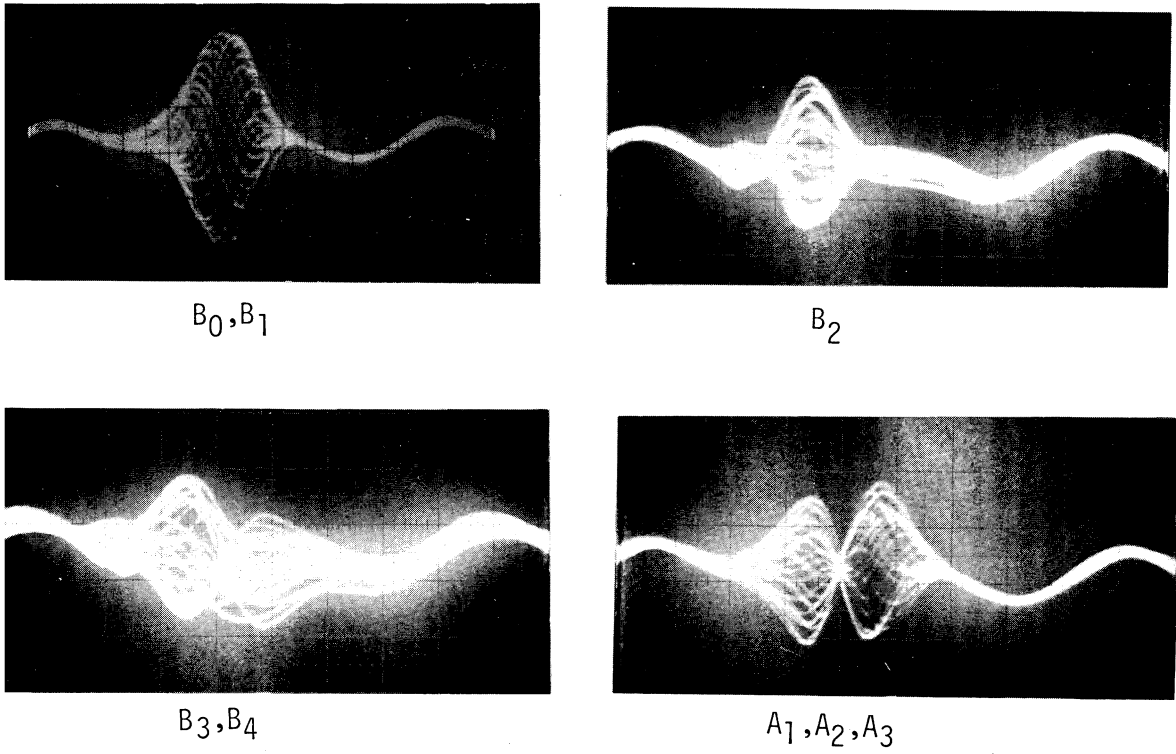
B_0, B_1

B_2

B_3, B_4

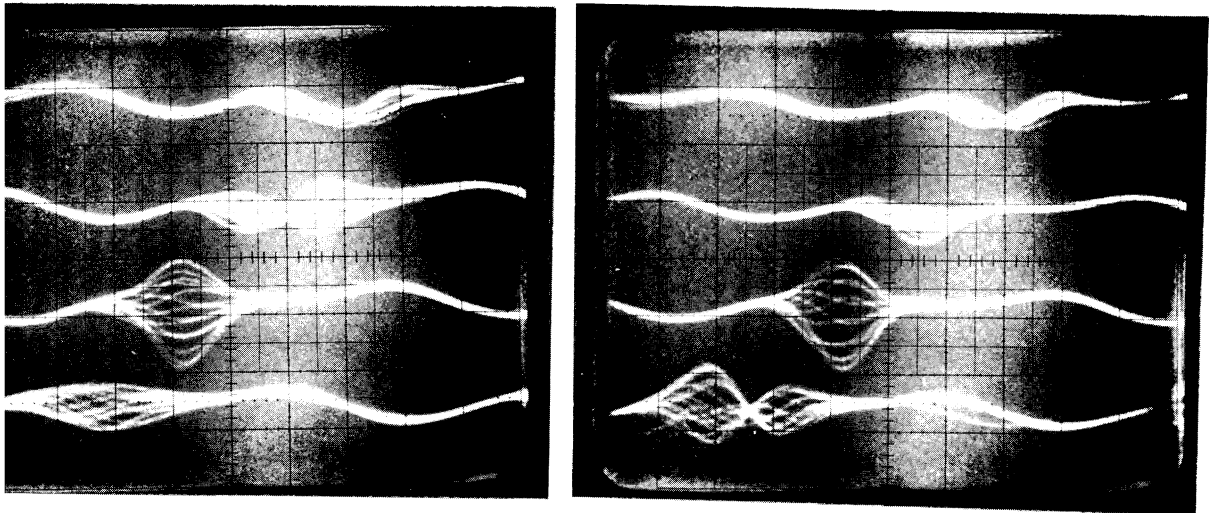A_1, A_2, A_3

FIGURE 15   Observed single modes.

FIGURE 16   Subsequent multi traces in the range 18 ∽ 21 msec with the interval 1 msec (from the bottom to the top).

change to various modes. The mode change has several patterns and the figure shows typical patterns. The expansion of Z_s with exponents, as in Eq. (3-20), does not show these modes explicitly but only phase shift.

iii) two kicker magnets According to Eq. (2-4), the resonance frequencies of the kicker magnet become approximately half when two kicker magnets are connected in series. Measured resonance frequencies are $\Omega_1/2\pi = 4.98$ MHz and $\Omega_3/2\pi = 14.0$ MHz, and the sharpness of the resonances is similar to that of the magnet K2. The buildup time calculated for this condition is shown as K2–K3 in Fig. 12. The β_{max} is large, around 19 msec. We have observed a weaker instability around 20 msec, as shown in Fig. 13-b.

The kicker magnet used for single-turn injection test is longer. Its resonance frequencies are $\Omega_1/2\pi = 6.0$ MHz and $\Omega_3/2\pi = 16.0$ MHz. The β_{max} calculated and shown with K1 in Fig. 12 is rather small. We have not observed any instability for this magnet.

5. DISCUSSION

According to Pellegrini and Sands, the inverse buildup time is proportional to $\zeta/\eta(4\mu^2 - 1)$, so if the mode $\mu = 0$ is stable, modes, $\mu = 1, 2,\ldots$ are unstable (and vice versa, depending on the sign of ζ/η). This criterion does not apply to the instability in the booster. We have observed the mode $\mu = 0$ and the modes $\mu = 1,2,3$ in the same condition.

Sacherer showed that the inverse buildup time is proportional to $Z_\perp(\omega_k)h_\mu(\omega_k - \omega_\zeta)$. The transverse impedance $Z_\perp(\omega_k)$ is large when $\omega_k (= (k + \nu)\omega_0)$

is equal to some resonance frequency. The Fourier transform $h_\mu(\omega_k - \omega_\zeta)$ of the bunch profile is large when $\omega_k - \omega_\zeta (= (k + \nu - q)\omega_0) \approx 0$. These things are similar to our results. The $Z_\perp(\omega_k)$ corresponds to H_{mk} and $h_\mu(\omega_k - \omega_\zeta)$ to $G_{\mu k}^\pm F_{\mu k}^\pm$. At present, H_{mk} is expressed explicitly and the results of the calculation agree with the observations, while $Z_\perp(\omega_k)$ is given only in a general form.[5]

We have thus derived a formula of the buildup time of the coherent transverse instability due to a kicker magnet whose termination is removed. The results explain quite well the observations of the buildup time and the oscillation mode and we therefore believe that the instability is correctly described.

ACKNOWLEDGEMENTS

REFERENCES

1. L.J. Laslett, V.K. Neil, and A.M. Sessler, *Rev. Sci. Instrum.* **36**, 436 (1965).
2. E.D. Courant and A.M. Sessler, *Rev. Sci. Instrum.* **37**, 1579 (1966).
3. C. Pellegrini, *Nuovo Cimento* **64A**, 477 (1969).
4. M. Sands, SLAC-TN-69/8 and SLAC-TN-69/10, (1969).
5. F. Sacherer, CERN/SI-BR/72-5, (1972).
6. Y. Kimura, Y. Miyahara, H. Sasaki, K. Satoh, K. Takata and K. Takikawa, Proc. of the 10th International Conf. on High Energy Accelerators, *Serpukhov* **2**, 30 (1977).
7. K. Takata, K. Tazawa, and Y. Kimura, KEK-76-21 (1977).